BOLETÍN DE LA SOCIEDAD ESPAÑOLA DE CERÁMICA Y VIDRIO XXX (2017) XXX–XXX

BOLETIN DE LA SOCIEDAD ESPAÑOLA DE
Cerámica y Vidrio
www.elsevier.es/bsecv

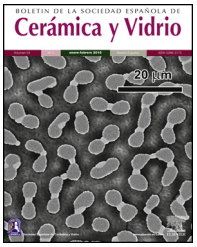

Review

Development and characterization of multi-element doped hydroxyapatite bioceramic coatings on metallic implants for orthopedic applications

Monika Furko[a,*], Viktor Havasi[b], Zoltán Kónya[b], Alina Grünewald[c], Rainer Detsch[c], Aldo R. Boccaccini[c], Csaba Balázsi[a]

[a] Hungarian Academy of Sciences, Centre for Energy Research, H-1121 Konkoly-Thegestr. 29-33, Budapest, Hungary
[b] University of Szeged, Department of Applied and Environmental Chemistry, Rerrich B. sqr 1, H-6720 Szeged, Hungary
[c] University of Erlangen-Nuremberg, Department of Materials Science and Engineering, Institute of Biomaterials, Cauerstr. 6, 91058 Erlangen, Germany

ARTICLE INFO

Article history:
Received 12 June 2017
Accepted 13 September 2017
Available online xxx

Keywords:
Coatings
Microstructure
Corrosion
Bioceramics

ABSTRACT

Multi-element modified bioactive hydroxyapatite bioceramic (mHAp) coatings were successfully developed onto surgical grade titanium alloy material (Ti6Al4V). The coatings were prepared by pulse current deposition from electrolyte containing adequate amounts of calcium nitrate and ammonium dihydrogen phosphate at 70 C. The pure HAp layer was doped and co-deposited with Ag, Zn, Mg, Sr ions. The biocompatible properties of layers were investigated by seeding osteoblast-like MG-63 cells onto the samples' surface. The biocompatible measurements revealed enhanced bioactivity of modified HAp compared to uncoated implant materials and pure bioceramic coating. The morphology and structure of coatings and cells were characterized by scanning electron microscopy (SEM), energy-dispersive X-ray spectroscopy (EDX) as well as FT-IR and XRD measurements. The biodegradable properties of samples were investigated by electrochemical potentiodynamic measurements.

* *Corresponding author.*
E-mail address: furkomonika@gmail.com (M. Furko).
http://dx.doi.org/10.1016/j.bsecv.2017.09.003

Please cite this article in press as: M. Furko, et al., Development and characterization of multi-element doped hydroxyapatite bioceramic coatings on metallic implants for orthopedic applications, Bol. Soc. Esp. Cerám. Vidr. (2017), http://dx.doi.org/10.1016/j.bsecv.2017.09.003

Desarrollo y caracterización de recubrimientos biocerámicos de hidroxiapatita dopados con multi-elementos en implantes metálicos para aplicaciones ortopédicas

Palabras clave:
Recubrimientos
Microestructura
Corrosión
Biocerámicas

RESUMEN

Se han desarrollado con éxito recubrimientos biocerámicos de hidroxiapatita bioactiva modificada con multi-elementos (mHAp) sobre soportes de titanio de grado quirúrgico (Ti6Al4V). Los recubrimientos se depositaron con la técnica de la corriente pulsada a partir de electrólitos con cantidades adecuadas de nitrato de calcio y dihidrogenofosfato de amonio a 70 °C. La capa de HAp pura se dopó y co-depositó con iones Ag, Zn, Mg,Sr. La biocompatibilidad de las capas se investigó mediante siembra de células de MG-63, similares a los osteoblastos, en la superficie de las muestras. Los resultados de los ensayos de biocompatibilidad revelaron una bioactividad mejorada de la HAp modificada en comparación con materiales de implante no revestidos y de revestimiento biocerámico puro. La morfología y estructura de los revestimientos y las células fueron caracterizadas mediante microscopía electrónica de barrido (MEB), espectrometría de dispersión de energía de rayos X (EDX), así como mediante mediciones de FT-IR y DRX. La biodegradabilidad de las muestras se investigó mediante ensayos potenciométricos dinámicos.

Introduction

Great efforts are made to improve the biocompatibility properties of commonly used metallic implant materials in orthopedic surgery. One solution can be applying bioactive coatings such as calcium phosphates. The phase, structure, composition and morphology of the CaP surfaces are important parameters that must be accurately controlled to influence their potential biofunctionality with respect to osteoblasts since interaction between calcium phosphate (CaP) thin layers and osteoblasts can be influenced by the outermost surface properties of those materials. Hydroxyapatite (HAp) has been extensively studied due to the structural and chemical similarities to the main inorganic constituent of bone tissues. However, it is well documented that biological hydroxyapatite, which forms the mineral phases of calcified tissues (enamel, dentin and bone), differ from pure and synthetically produced HAp [1–3]. Biological apatite consists of a mixture of calcium phosphate phases, such as tricalcium phosphate (TCP), carbonated hydroxyapatite (CHA) and calcium-deficient hydroxyapatite (CDHA). In this regard, synthetic HAp exhibits a Ca/P ratio of 1.67, while biological apatite deviates significantly from this value and its Ca/P ratio is known to be as low as 1.5. One promising way to modify the osteoblastic response of HAp coatings, both in vitro and in vivo, could involve the use of substituted HAp, incorporating different ions, such as silicon [3], magnesium [5], zinc [6], silver [7], strontium [8] into the HAp lattice. Numerous research works on the use of these substituted materials can be found in the literature [3–11]. On the other hand, deep infection of megaprostheses is still a serious complication in orthopedic surgery. Bacterial adhesion and biofilm formation on these alloys can easily cause various human diseases after surgery [12]. Removing bacteria in a biofilm is impossible and a local or systemic antibiotic treatment is not effective. Therefore, the inhibition of bacterial adhesion is the most critical step in preventing implant-associated infections [13].

In view of the problem of bacterial resistance to antibiotics and antiseptics, nano-structured silver-containing coatings may be an effective way to prevent device related infections, because its high and permanent antimicrobial activity combines with a remarkably low human toxicity [14–16]. Silver and in particular the free silver ion is well known for its broad-spectrum antimicrobial activity and its low toxicity to mammalian cells, but still allows for the independent use of therapeutic antibiotics [13–16]. Strontium has been shown to have the dual benefit of promoting bone formation and reducing bone resorption. Furthermore, it has been shown that strontium has the ability to enhance pre-osteoblastic cell replication and can stimulate the formation of new bone through osteogenesis and differentiation into osteoblasts and has the ability to inhibit the activity of osteoclasts [17–22]. Mg^{2+} doping can enhance the osteoblast adhesion strength as compared to pure HAp since incorporation of Mg into pure calcium HAp makes it closer to the natural bone [23] while the Zn content can promote the wound healing process after implantation.

One of the most promising and cheapest methods to deposit coatings onto metallic substrates is the electrodeposition, more specifically pulse current deposition. The main advantages of applying pulse current instead of direct current are that more homogeneous, uniform coatings with smaller grain size can be achieved thus improving the mechanical and chemical properties of coatings. So far, many research works have been performed using this novel method for layer deposition [24–30]. Gopi et al. [24] have prepared minerals doped hydroxyapatite coating by pulse current on and off time in seconds (from 1 s to 4 s) and investigated the effect of parameter change. Wang et al. [25], however, applied pulse-reverse current for electrodeposition. In their experiments the positive and reverse pulse duty cycles were 0.1 and 0.5, and the

Please cite this article in press as: M. Furko, et al., Development and characterization of multi-element doped hydroxyapatite bioceramic coatings on metallic implants for orthopedic applications, Bol. Soc. Esp. Cerám. Vidr. (2017), http://dx.doi.org/10.1016/j.bsecv.2017.09.003

positive and reverse plating times were 10 and 2 ms. They found that well adherent coating could be achieved by this method without any post-treatment. The morphology of the such prepared coating was mainly plate-like with thickness of around 100 nm. In a more recent study, Marashi-Najafi et al. [26] reported hydroxyapatite coating deposition onto Nitinol superelastic alloy by pulse current with duty cycle of 0.2 at different current densities. They also studied the effect of electrolyte concentration on the morphology of coatings and they revealed that the structure changed from needle like to plate like as the electrolyte concentration decreased. In addition, it is worthwhile to mention that in some research works voltage (pulsed or direct) was used for deposition instead of current, according to the authors' reports [27–30].

In our present research work multi-element (Ag, Zn, Sr and Mg) doped hydroxyapatite coatings have been prepared by combination of pulse current electrodeposition method and surface post-treatment. The morphology and structure of layers have been studied with SEM-EDX measurements. Layers have been also characterized by FT-IR spectroscopy and X-ray diffraction measurements. The biocompatible properties of layers have been assessed using MG-63 osteoblast-like cells and the biodegradable characteristics of samples have been tested in simulated body fluid by electrochemical method.

Experimental

Preparation of pure and substituted calcium phosphate/hydroxyapatite coatings

Titanium alloy (Ti6Al4V, ISO5832-3, Protetim Ltd.) discs (10 mm × 1 mm) were used as substrates. One side of each disk was roughened using a sandblasting procedure with a 180-grit aluminum oxide media (according to the standard procedure applied by the manufacturer similarly than in the cases of commercial implant materials). This surface pre-treatment is necessary to enhance the adherence of layers.

IGTV-4i/6t type pulse current generator was used to prepare the different bioceramic coatings. In the pulse current waveform t_{on} is the time when current flows and t_{off} is the relaxation time when the current is zero. Applying t_{off} time in pulse current deposition gives the system time to recover during the relaxation periods. The electrodeposition process was carried out in a two-electrode cell under normal atmospheric conditions, where the anode was a platinum sheet and the metallic implant disk was used as a cathode. The deposition parameters are summarized in Tables 1 and 2. The thickness of layers was around 1–2 μm in all cases (Fig. 1). The morphological properties of the layers were studied by SEM and FIB measurements with LEO 1540XB Crossbeam workstation. The beam parameters in SEM imaging mode were 5 keV beam energy and 30 μm aperture size, Everhart-Thornley and InLens secondary electron detectors were used. The ion beam parameters in FIB milling mode were 30 kV accelerating voltage and 5 nA beam current. For SEM/FIB measurements the samples were tilted at 36 angle. The electron beam parameters for the EDX were 8 and 16 keV beam energy. A Röntec Si(Li) detector and the Bruker Esprit 1.9 software had been used for the EDX measurements.

Table 1 – Electrodeposition parameters for obtaining pure hydroxyapatite layers.

Electrochemical deposition	
Electrolyte	Concentration/gL
$Ca(NO_3)_2$	115.6
$NH_4H_2PO_4$	33.30
H_2O_2 (30%)	10 ml
Deposition parameters	
t_{on}/ms	1
t_{off}/ms	10
i_p/A cm^{-2}	5
Bath temperature/°C	70
pH	4.5
Deposition time/s	3
Surface treatment after deposition	1 M NaOH solution, 70 °C, 2 h

Table 2 – Electrodeposition parameters for obtaining modified HAp layers.

Electrodeposition	
Electrolyte	Concentration/gL
$Ca(NO_3)_2$	115.6
$Mg(NO_3)_2$	2.56
$Sr(NO_3)_2$	2.10
$NH_4H_2PO_4$	33.30
H_2O_2 (30%)	10 ml
Deposition parameters	
t_{on}/ms	1
t_{off}/ms	10
i_p/A cm^{-2}	5
Bath temperature/°C	70
pH	4.5
Deposition time/s	3
Surface treatment after deposition	Soaking in solution containing 0.01 M $Zn(NO_3)_2$ and 0.0025 M $AgNO_3$ for 24 h and afterward in 1 M NaOH solution at 70 °C for 2 h with subsequent heat treatment at 150 °C for 2 h.

FT-IR characterization

To record FT-IR absorption spectra of investigated samples, specular reflection technique was employed. All infrared spectra of the samples were recorded on a Bruker Vertex 70 FT-IR spectrometer coupled with Hyperion 2000 IR microscope with 15× (NA = 0.4) specular reflection objective. Spectra were recorded over the range of wave number 4000–400 cm^{-1} at room temperature using 128 scans at 2 cm^{-1} resolution.

X-ray diffraction measurements

The crystal structures of the samples were investigated using X-ray diffraction. XRD spectra were recorded at room temperature by Rigaku MiniFlex II diffractometer (Cu K_α radiation source, 0.15418 nm) equipped with a high count DTEX II detector and operated at 40 kV and 40 mA. The diffraction patterns were collected over a 2θ range from 10° to 60° with 1°/min steps using flat plane geometry.

Please cite this article in press as: M. Furko, et al., Development and characterization of multi-element doped hydroxyapatite bioceramic coatings on metallic implants for orthopedic applications, Bol. Soc. Esp. Cerám. Vidr. (2017), http://dx.doi.org/10.1016/j.bsecv.2017.09.003

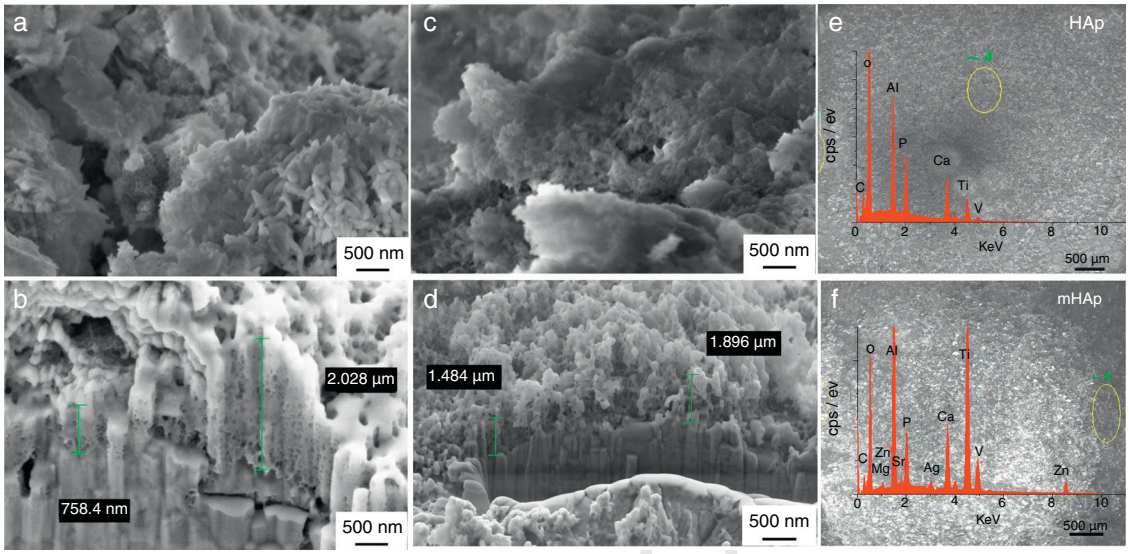

Figure 1 – SEM and SEM/FIB measurements on pure HAp layer (a, b) and on multi-ion modified HAp (c, d) as well as EDX spectra on HAp (e) and mHAp (f).

Electrochemical corrosion measurements

The potentiodynamic polarization studies were carried out with Zahner IM6e electrochemical workstation (Zahner, Germany). In the electrochemical measurements conventional three-electrode cell was used. The working electrode was a metallic implant disk (19 mm) with and without coatings and platinum net and Ag/AgCl/KCl_{sat} electrodes were used as counter electrode and reference electrode, respectively. The potentiodynamic polarization curves were recorded with 1 mV/s scanning rate. Simulated body fluid was used as an electrolyte for all the electrochemical experiments, which has ion concentrations nearly equal to those of human blood plasma and is buffered at pH 7.40 with 50 mM trishydroxymethylaminomethane and 45 mM hydrochloric acid. The composition of simulated body fluid can be seen in Table 3. By measuring the corrosion properties of samples it is possible to trace their biodegradation properties. All the electrochemical characterizations were carried out at temperature of 37 °C to simulate body conditions.

Table 3 – Composition of simulated body fluid [31].

Reagent	Amount (g/L)
Sodium chloride	7.996
Sodium bicarbonate	0.350
Potassium chloride	0.224
Potassium phosphate trihydrate	0.228
Magnesium chloride hexahydrate	0.305
1 M hydrochloric acid	40 mL
Calcium chloride	0.278
Sodium sulfate	0.071
Tris (hydroxymethyl) aminomethane	6.057

Biocompatible measurements on pure and modified hydroxyapatite layers

Cell culture

Cells used for the experiments are represented by MG-63 cell line (Sigma–Aldrich, Germany), which is a line of human osteoblast-like cells. Cells were grown on 75 ml flasks and were detached by tripsin. Medium was DMEM (Dulbecco's Modified Eagles Medium) with 10% of FBS (fetal bovine serum, containing growth factors and nutrients to support cell growth) and 100 U/ml penicillin and 100 µg/ml streptomycin to minimize the risk of infections. The cultures were maintained at 37 °C, 5% CO_2 in a humidified atmosphere in incubator (New Branswick Galaxy 170S). The culture media were changed in every three days. The cells were counted in a Neubauer chamber.

Cell viability measurements with WST-8 reagent

For cell viability measurements the samples were put in a 24-well microtiter plate and 1 ml of cell suspension at concentration of 10,000 cells/mL was seeded onto the surface of each samples. The same amount of culture medium with cells without samples was used as control. After a cultivation period of 2, 7 and 14 days, the culture media was removed from the 24 well culture plate and the cells were washed with sterile PBS. After washing, 1 mL of DMEM medium containing 1% WST-8 reagent were added to the wells and it was incubated for 3.5 h. The incubation period was followed by spectrophotometric assay of colored product. During this incubation period viable cells convert WST-8 to a water soluble formazan dye. The specific absorbance of formazan dye (at 450 nm) in the MTP can be done with an ELISA plate reader (PHomo Autobio Anthos Mykrosystem GMbh, Germany). The absorbance directly correlates with the cell number.

ALP activity measurements

ALP enzyme activity was measured after 6 and 14 days of incubation in order to characterize the osteoblastic activity of the MG-63 cells. The cells were lysed with a cell lysis buffer which contains 20 mM TRIS buffered solution (Merck) with 0.1 wt% Triton X-100 (Sigma, Germany), 1 mM $MgCl_2$ and

Please cite this article in press as: M. Furko, et al., Development and characterization of multi-element doped hydroxyapatite bioceramic coatings on metallic implants for orthopedic applications, Bol. Soc. Esp. Cerám. Vidr. (2017), http://dx.doi.org/10.1016/j.bsecv.2017.09.003

Table 4 – Elemental analysis of HAp and mHAp coatings derived from EDX measurements.

	Atomic percent (%)										
Spectrum	C	O	Al	Ti	V	Ca	P	Ag	Zn	Mg	Sr
HAp	11.68	56.18	8.74	9.38	0.47	8.53	5.02	–	–	–	–
mHAp	12.43	56.38	9.77	13.88	0.17	4.08	2.62	0.34	0.06	0.19	0.08

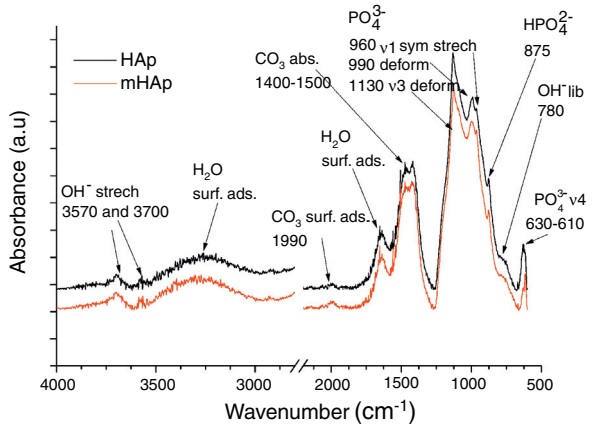

Figure 2 – FT-IR spectra of HAp coating and modified HAp coating.

0.1 mM $ZnCl_2$. The cell lysate was incubated with a reacting solution containing 0.1 M Tris solution, 2 mM $MgCl_2$ and 9 mM p-Nitrophenylphosphate for 120 min. After incubation absorption was measured at 405 nm using a spectrometer (Specord 40).

Calcein staining

For staining the live cells, acetoxymethyl (AM) ester (Calcein, Molecular Probes, Germany) was used which is a fluorescent indicator. The cell distribution growth on the sample surface was analyzed using florescent microscope (FM, Scope. A1, Carl Zeiss). After the cultivation period of 48 h, the adherent cells were fixed with 3.7 vol% paraformaldehyde for 10 min and permeabilised with 0.1 vol% Triton X-100 (in PBS) for 10 min at room temperature.

DAPI (4′,6-diamidino-2-phenylindol) staining

The nuclei of fixed cells were stained with the fluorescence dye 4′,6-diamidino-2-phenylindol (DAPI RotiVR-Mount FluorCare). For staining of the samples, the matrices were incubated 15 min in the dark in DAPI-solution (2 mL DAPI-stock solution in 1 mL DAPI buffer). After staining ward, the matrices were washed three times in PBS to eliminate the background. The nuclei were imaged by the fluorescence microscope with blue filter.

Morphological characterization of MG-63 cells by SEM imaging

The samples, seeded and cultured with MG-63 cells for 2 days were washed with PBS, fixed with a solution containing 3 vol% glutaraldehyde (Sigma, Germany) and 3 vol% paraformaldehyde (Sigma, Germany) in 0.2 M sodium cacodylate buffer (pH 7.4), and thoroughly rinsed with PBS for SEM analysis (Auriga CrossBeam, Carl Zeiss Microscopy GmbH, Germany). All samples were dehydrated in ethanol, stored in 99.8 vol% ethanol and critical-point dried (EM CPD300, Leica, Germany).

Statistics

Results are presented using the mean value and standard deviation of four replicates of each sample type. All results were normalized to MG-63 cells growth on a well plate (REF = 100%). The differences in analysis parameters between the different samples investigated were evaluated by one-way analysis of variance (ANOVA). The level of the statistical significance was defined at $p < 0.05$ (Origin 8.6, Origin Lab Corporations, USA). The significance level was set as $^{*}p < 0.05$, $^{**}p < 0.01$ and $^{***}p < 0.001$. For the comparison of the mean values the Tukey test was used.

Results and discussion

Morphological investigation

Fig. 1 shows the SEM and FIB measurements on HAp layer and on modified HAp coating. It can be seen in Fig. 1(a) that the pulse electrodeposited HAp coating after surface treatment in 1 M NaOH solution has mainly small needle-like and larger rod-like particles with length of 100–200 nm and with diameter of 20–50 nm. The Ca/P elemental ratio in this case is 1.78 (Table 4) which can indicate mainly hydroxyapatite crystals in the layer. The SEM-FIB cross sectional image (Fig. 1b) revealed that the layer has a very porous, sponge-like structure and its thickness is not uniform. The thickness of layer varied between 700 nm and 2 μm, depending on the site of samples.

The metal ion-modified HAp layer (Fig. 1b) shows similar morphology, however, in this case flake-like particle agglomerations can also be observed. The SEM-FIB cross sectional image shows similarly porous structure with layer thickness of 1–2 μm. On the corresponding EDX spectra, weak peaks of Ag, Zn Sr and Mg element signals are also visible proving the presence and incorporation of metallic ions and particles in HAp layer. The elemental analysis reveals the Ca/P elemental ratio to be 1.55 which can indicate the HAp crystal structure disruption or the presence of other CaP phases as impurities. However, this small amount of other calcium phosphate phase could not be detected by XRD measurement due to the detection limit (Fig. 3). It is visible on EDX spectra that Ti and Al and V peaks also appear because the applied electron beam excited the substrate material also due to the very thin and inhomogeneous coating. The appearing very weak signal of C on the EDX spectra might indicate the presence of some carbonate impurities. This result is in good accordance with the FT-IR measurements in Fig. 2.

Please cite this article in press as: M. Furko, et al., Development and characterization of multi-element doped hydroxyapatite bioceramic coatings on metallic implants for orthopedic applications, Bol. Soc. Esp. Cerám. Vidr. (2017), http://dx.doi.org/10.1016/j.bsecv.2017.09.003

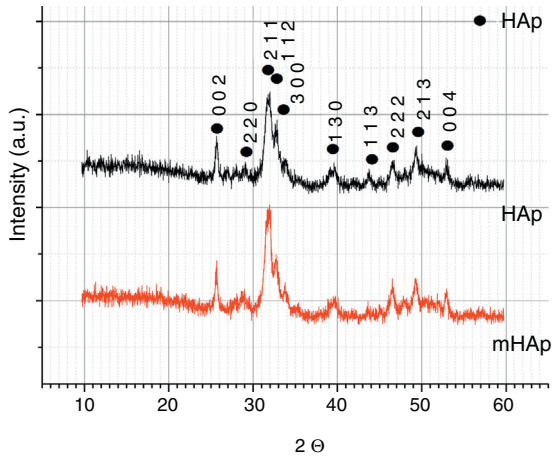

Figure 3 – XRD measurements on HAp coating and on modified HAp coating.

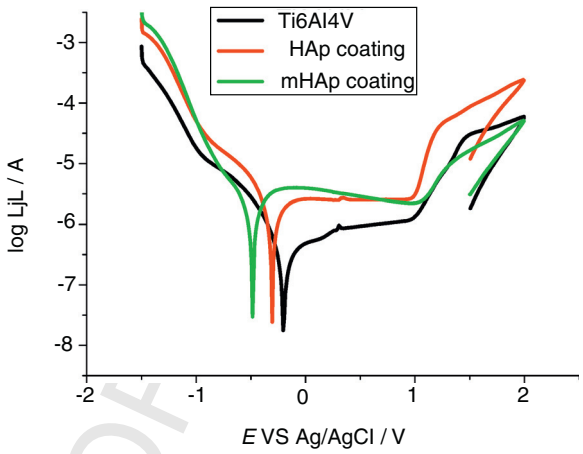

Figure 4 – Potentiodymanic polarization curves of uncoated Ti6Al4V alloy (black line), of HAp coating (blue line) and of mHAp (green line) recorded after two weeks immersion in SBF solution at 37 °C. The potential scanning rate is 1 mV/s.

FT-IR analysis of pure and modified calcium phosphate layers

As Fig. 2 shows, the FT-IR spectra are very identical for both coatings. On the spectra of HAp and mHAp samples peaks at 627, 960, 990 and 1130 cm^{-1} are related to PO_4^{3-} anionic group content, while the wide absorption peak in the 1400–1500 cm^{-1} region is connected to absorbed CO_3^{2-} content of HAp phase [32]. Weaker overlapped peaks at 875 cm^{-1} can be related to HPO_4^{2-} content, suggesting the presence of a minor carbonated hydroxyapatite (cHAp) phase in coatings. However, the slightly higher absorption of OH^- groups (OH^- stretch vibration) at 3700 cm^{-1} in the case of mHAp coating might be explained by some elimination of cHAp phase from HAp owing to the incorporation of doping elements. In addition, slight signs of adsorbed water bands also appear on spectra from 3600 cm^{-1} to around 2600 cm^{-1} and at 3570 cm^{-1}.

X-ray diffraction analysis

The XRD patterns of pure and doped HAp samples are shown in Fig. 3. Both spectra shows characteristic peaks of HAp at 2 = 31.7° (2 1 1), 32.9° (3 0 0), 25.88° (0 0 2) in accordance with the JCPDS file 09-0432. The broad XRD peaks for HAp indicate its nanocrystallinity. In the case of multi-ion modified HAp, very similar peaks can be observed. No other CaP phases or phosphate impurities can be detected on the spectra owing to the detection limit and the components' very low concentrations. In our case, there is no visible line shifting, peak broadening and changing in peak intensity when metallic ions are added to the hydroxyapatite coating. However, several studies reported line shifting to higher 2 values due to the replacement of larger sized Ca^{2+} (0.099 Å) ions with smaller sized Mg^{2+} (0.69 Å) ions and Zn^{2+} (0.77 Å) ions [33–35]. In other research work, Ziani et al. found broadening of the peaks due to the reduction in the crystallite size and increase in the lattice disorder, which they attributed to the Mg^{2+} substitution in the HAp lattice [36]. On the other hand, the substitution of strontium and silver can cause phase shifting to lower 2θ indicating an increase in the lattice parameters, which can be attributed to the higher ionic radius of Sr (1.13 Å) and Ag (1.15 Å), as compared to Ca^{2+} [37].

Table 5 – Electrochemical parameters: passive current density (j_p), corrosion potential (E_{corr}) and corrosion current (j_{corr}) values derived from the potentiodynamic curves in Fig. 4.

Sample	j_p/A cm^{-2}	j_{corr}/A cm^{-2}	E_{corr} vs Ag/AgCl/mV
Ti6Al4V	0.91	0.26	−190
HAp coating	2.57	1.04	−295
mHAp coating	3.30	1.51	−486

Corrosion characterization by electrochemical potentiodynamic measurements

Fig. 4 demonstrates the potentiodynamic curves of implant material (Ti6Al4V) and HAp coating and modified HAp coating. The curves were recorded after two weeks immersion in SBF solution.

As Fig. 4 reveals, large anodic passive regions can be observed on the anodic branches of potentiodynamic curves in all cases with small passive current densities (j_p) and the shapes of potentiodynamic curves of all samples is quite similar. In the case of uncoated implant material the onset of this passive region is around +100 mV vs Ag/AgCl and the passive film breakdown potential is at +980 mV. The passive region on potentiodynamic curves of pure HAp coating became slightly wider after two weeks of immersion than that for uncoated sample, it starts at around −120 mV vs Ag/AgCl and its breakdown potential is similarly at around +980 mV. On the other hand, the widest passive region is observed in the case of mHAp coating, spreading from −280 mV to around +1 V vs Ag/AgCl. The very large slopes of anodic and cathodic branches of curves indicate mixed kinetic and diffusion controlled electrode processes for all samples.

Please cite this article in press as: M. Furko, et al., Development and characterization of multi-element doped hydroxyapatite bioceramic coatings on metallic implants for orthopedic applications, Bol. Soc. Esp. Cerám. Vidr. (2017), http://dx.doi.org/10.1016/j.bsecv.2017.09.003

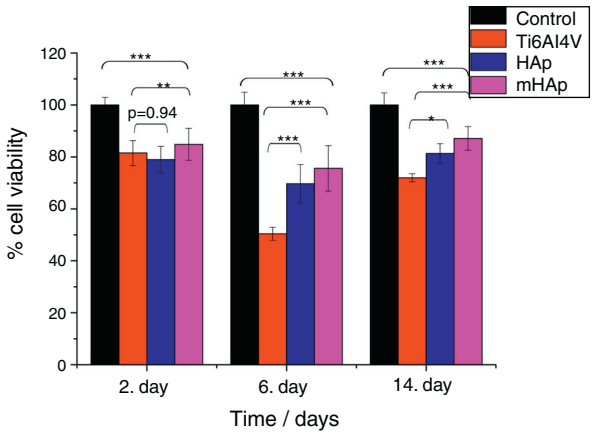

Figure 5 – Cell viability percentage on the investigated samples compared to positive control. Positive control: MG-63 cells were grown in well plates without samples. The level of thestatisticalsignificance is given by *p*-values as compared to control and titanium substrate. All samples were measured in 6 replicate and calculated the mean values ± standard deviation.

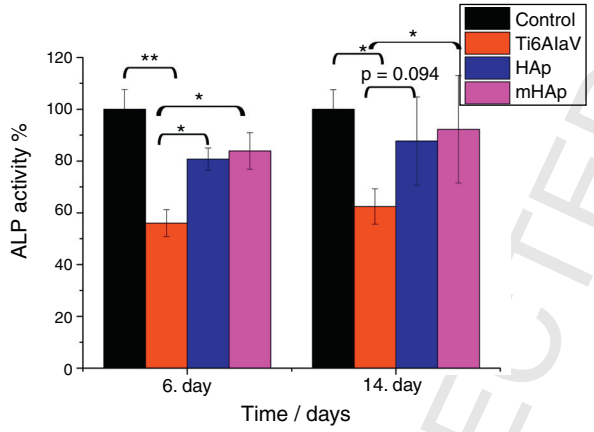

Figure 6 – ALP expression percentage on the investigated samples compared to positive control. Positive control: MG-63 cells were grown in well plates without samples. The level of the statistical significance is given by *p*-values as compared to control and titanium substrate. All samples were measured in 6 replicate and calculated the mean values ± standard deviation.

The electrochemical parameters, such as passive current densities, corrosion current densities and corrosion potentials of different samples are summarized in Table 5.

It is visible that the titanium alloy substrate possesses the lowest passive current density (0.91 A cm^{-2}), while the highest value belongs to multi-element doped HAp coating (3.30 A cm^{-2}). On the other hand, it can also be observed on the anodic branch of potentiodynamic curves that while the passive currents of mHAp samples slightly decrease with potential scan, the passive currents of substrate material and HAp coating are stable and hardly change till the breakdown potential.

The corrosion current density (j_{corr}) values and corrosion potentials (E_{corr}) can be obtained by the intersection of lines extrapolated to the cathodic and anodic branch of potentiodynamic curves in the Tafel region (±50 mV from corrosion potential). The titanium alloy has the noblest corrosion potential and lowest corrosion current density which denotes its highest corrosion stability. On the other hand, the most negative E_{corr} and the highest j_{corr} values belong to the mHAp samples. This result can prove that during immersion in physiological solution, dissolution processes of different doping elements as well as calcium phosphate components can occur.

There are several research works investigating the degradation processes of hydroxyapatite coatings prepared by different methods. It is reported that the porous characteristic (size and number of pores present in the coating) of calcium phosphate coatings significantly affects the corrosion/dissolution rate of hydroxyapatite. The coatings with smaller and fewer pores proved to be more corrosion resistant than coatings with higher degree of porosity because the former can provide better barrier property [38–40].

Zhang et al. [32] stated that the corrosion mechanism of HAp coating with pores involves hydrogen ion (H^+) generation at the interface where corrosion occurs, thus decreasing the local pH value, and then causes subsequent dissolution of HAp in the high H^+ concentration area. The dissolution rate of HAp increases with decreasing pH.

Biocompatible measurements on samples

Cell viability measurement with WST-8 assay

Fig. 5 shows that in all culture period the mHAp sample had the highest cell viability values, after 2 days it was 85% while after two weeks it increased to around 90% compared to positive control.

The cell viability percentages were 78% and 85% after 2 days, 81% and 90% after 2 weeks of culture on pure HAp and multi-ion modified HAp coatings, respectively. For uncoated titanium, the viability was 81% at 2nd day and it decreased to 71% at 14th day. After 2 days of culture, the differences between the cell viability values were not statistically significant for HAp compared to titanium substrate (p value was 0.94), while the difference between Ti alloy and mHAp was statistically different ($p < 0.01$). It is visible that there is a slight decrease in cell viability for each sample after one week of incubation. This phenomenon can be explained by cell differentiation. Several researchers proved that when cells are in the state of differentiation, they show less metabolic activity resulting in lower viability values [41,42].

After 2 weeks of culture in DMEM medium the difference between the cell viability on HAp and on mHAp samples become more significantly higher than those for uncoated substrate, indicating the good biocompatible/bioactive properties of both hydroxyapatite layers. It is also visible that the multi-element modification advanced the biocompatibility of sample. The differences between the cell viabilities of samples in this time point were all statistically highly significant ($p < 0.001$). In addition, it is well known that hydroxyapatite coating facilitate the attachment and growth of osteoblastic cells owing to its high hydrophilic property [43,44].

Please cite this article in press as: M. Furko, et al., Development and characterization of multi-element doped hydroxyapatite bioceramic coatings on metallic implants for orthopedic applications, Bol. Soc. Esp. Cerám. Vidr. (2017), http://dx.doi.org/10.1016/j.bsecv.2017.09.003

Alkaline phosphatase activity measurements

ALP is one of the first osteoblastic markers. Since the osteoblast-like human MG-63 cell line is capable to produce some osteogenic markers such as alkaline phosphatase and osteocalcin [45]. In our present study ALP expression of cells seeded on the surface of different samples and on culture well plate as reference was evaluated.

It is visible in Fig. 6 that the ALP expression is higher by around 25% and 30% for pure HAp and multi-ion doped HAp, respectively, after 6 and 14 days of culture than that for uncoated substrate. The level of ALP activity increased with culturing time. After 6 days of immersion, the ALP values of both HAp and mHAp were statistically different ($p < 0.05$) compared to uncoated substrate, while there was no statistically difference between the calcium phosphate coatings and the control group. At the 14th day of culture, only the ALP values of mHAp compared to Ti alloy and ALP expression of control compared to Ti alloy were statistically different ($p < 0.05$). It is visible that the highest ALP expression belongs to mHAp sample. On the other hand, the differences between HAp and mHAp as well as between titanium substrate and HAp are not statistically different, in the latter case the p value is 0.094. Our findings are in good agreement with reports from literature where Zhao et al. [46] studied the effect of magnesium-substituted nano-hydroxyapatite coating on implant osseointegration. In their research they found that the magnesium substituted HAp had higher ALP activity by two times than that of without magnesium content after 7 days of culture. Yang et al. [47] investigated the biocompatibility of Zn substituted hydroxyapatite on Murine preosteoblast cell (MC3T3-E1) cell line. They reported significant increase in cell proliferation and ALP activity on day 7, and osteocalcin production ($p < 0.05$) were also observed for Zn^{2+}-containing HAp-coated surfaces on day 14. The coatings were prepared by electrochemical process and the Zn was present in the Zn-HAp coatings at a Zn/(Ca-Zn) molar ratio of 1.04%. Bueno et al. [48] studied the effect of Sr substitution in HAp nanocomposite on the differentiation of OFCOLL II osteoblasts. Other literature report showed that the presence of strontium in the HAp structure (SrHAp) seems to cause important effects in osteoblast and osteoclast growth and also favors the increase of osteoblast ALP activity [49]. Thian et al. [50] investigated the effect of apatite nanocrystals on the osteoblast behavior of human osteoblast (HOB) cells and they found that the ALP activity of cells growing on phase-pure apatite nanocrystals was detectable only after 5 days of culture.

Calcein/DAPI staining

Direct fluorescence staining of calcein and nucleus (DAPI) of MG-63 cells cultured for 2 days on titanium alloy, HAp and mHAp coatings as well as on control group (well plates) are shown in Fig. 7.

Calcein fluorescent staining is generally used to indicate intracellular esterase activity present in viable cells. Dense and evenly dispersed multi-layered cells with large nuclei were observed for all samples, however, in the case of HAp and mHAp coated samples there were larger number of living cells. The shape of cells mainly elongated and polygonal which indicates well adhered, spreading and proliferating cells.

MG-63 cell morphology study

The expression of the phenotype of osteoblast-like cells (MG-63) was studied by SEM after incubation on uncoated titanium

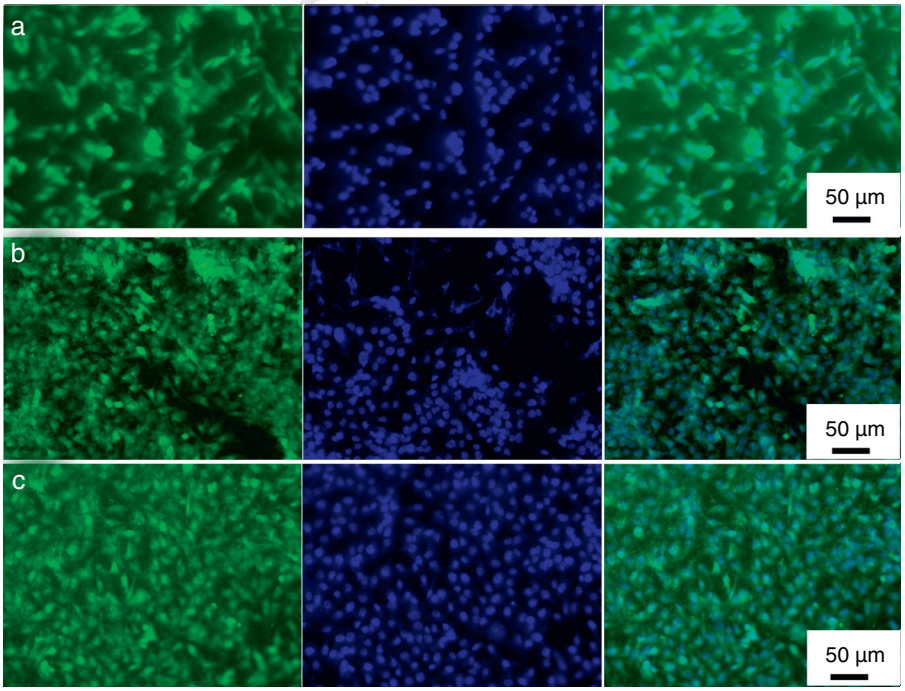

Figure 7 – Fluorescence microscopy images of calcein-AM (green fluorescent) and nucleus (with DAPI, blue fluorescent) and merged images of Mg-63 cells cultured for 2 days in DMEM medium on different samples such as titanium alloy (a) HAp (b) and mHAp (c) coatings.

Please cite this article in press as: M. Furko, et al., Development and characterization of multi-element doped hydroxyapatite bioceramic coatings on metallic implants for orthopedic applications, Bol. Soc. Esp. Cerám. Vidr. (2017), http://dx.doi.org/10.1016/j.bsecv.2017.09.003

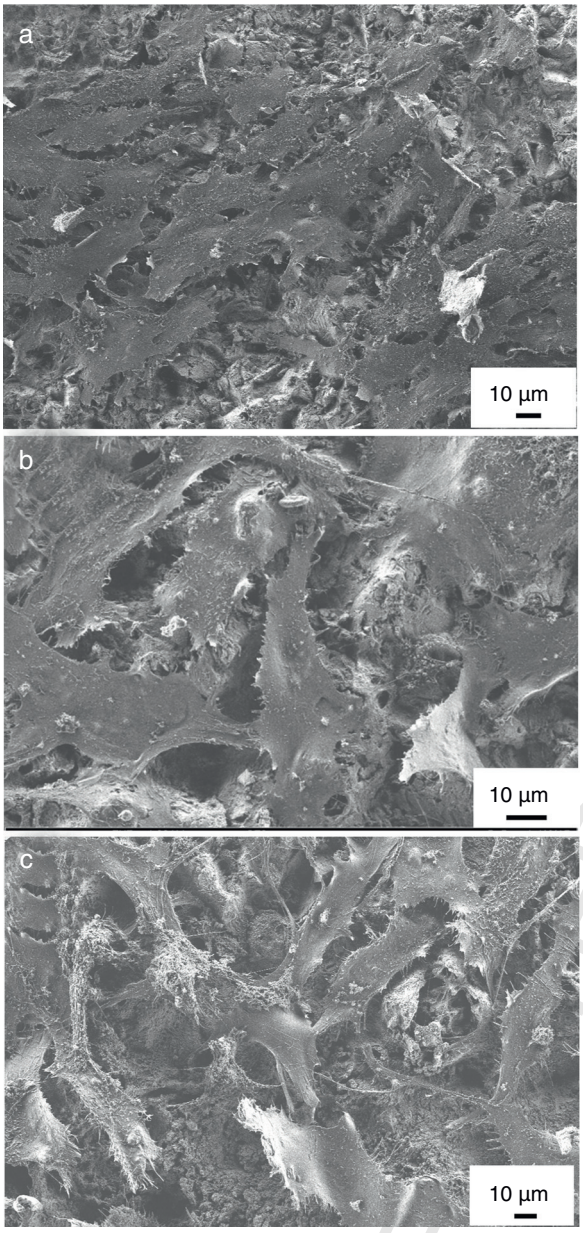

Figure 8 – SEM images on MG-63 cells grown on titanium substrate (a) on HAp coating (b) and on mHAp coating after 2 days of culture in DMEM medium.

alloy, on pure HAp coating and on ion-modified HAp coatings for 48 h. It is obvious that the phenotype of MG-63 osteoblast-like cells were well-expressed and cell were spreaded on the surfaces of all samples and were in flattened form. The shape of cells mainly polygonal with filopodia or very thin extensions. The cells covered the coated samples' surfaces in a thick continuous monolayer and the MG-63 started to form also a multilayer in some areas of the sample. On the other hand, in the case of uncoated substrate, the coverage was not perfect. In some places the surface of substrate is also visible beside the cells (see in Fig. 8a). The number and density of cells as well as the extent of spreading seemed to be a little higher in the case of calcium phosphate coated samples than for uncoated substrate. Nevertheless, there is not much visible difference in cell morphology in the case of both HAp and mHAp coated samples. These results might confirm that the coating can advance cell adherence thus promoting cell proliferation and prove the results from Calcein/DAPI staining.

Conclusion

The SEM analysis revealed that the morphology of HAp and mHAp coatings was mainly needle-like in nanometre size. The cross section analysis (FIB) showed the coatings to be in highly porous, sponge-like structure, which resembles the structure of natural bone. The EDX elemental analysis confirmed that the ions doped HAp coating contained Ag, Zn, Sr and Mg elements also in under 1 At% along with the calcium and phosphorous elements. The FT-IR spectra showed similar characteristic peaks of PO_4^{3-} and OH^- anionic groups of calcium phosphate phases and revealed carbonate impurities in both samples. The XRD measurements also confirmed that the coating consist of mainly nanocrystalline hydroxyapatite phase and there was no visible line shifting, peak broadening and changing in peak intensity when metallic ions were added to the hydroxyapatite coating. According to the corrosion measurements, the corrosion resistances of pure HAp and multi-ion doped HAp were lower than that of uncoated substrate due to the highly porous characteristic of layers.

The biocompatible tests showed that the cell viability values increased significantly in the cases of both HAp and mHAp samples compared to bare implant materials and the highest values were measured in the case of mHAp. The Calcein and DAPI staining of samples revealed dense, multi-layered, well adhered living cells on all samples with normal morphology. The in vitro results presented here support that HAp and multi-ion doped HAp coatings advance the growth of MG-63 osteoblast-like cells.

Acknowledgements

The authors would like to acknowledge the financial support of JECS Trust and the authors are grateful for the SEM-FIB/EDX measurements performed by Levente Illés (MTA-EK, Hungary).

REFERENCES

[1] L. Sun, C.C. Berndt, K.A. Gross, A. Kucuk, Material fundamentals and clinical performance of plasma-sprayed hydroxyapatite coatings: a review, J. Biomed. Mater. Res. B: Appl. Biomater. 58 (2001) 570–592.
[2] A.C. Tas, Combustion synthesis of calciumphosphate bioceramic powders, J. Eur. Ceram. Soc. 12 (2000) 2389–2394.
[3] E.S. Thian, J. Huang, S.M. Best, Z.H. Barber, W. Bonfield, Surface modification of magnetron-sputtered hydroxyapatite thin films via silicon substitution for orthopaedic and dental applications, Surf. Coat. Technol. 205 (2011) 3472–3477.
[4] S.V. Dorozhkin, M. Epple, Biological and medical significance of calcium phosphates, Angew. Chem. Int. Ed. 41 (17) (2002) 3130–3146.
[5] S. Ziani, S. Meski, H. Khireddine, Characterization of magnesium-doped hydroxyapatite prepared by sol–gel process, Int. J. Appl. Ceram. Technol. 11 (2014) 83–91.

[6] N.A. Trujillo, R.A. Oldinski, H. Ma, J.D. Bryers, J.D. Williams, K.C. Popat, Antibacterial effects of silver-doped hydroxyapatite thin films sputter deposited on titanium, Mater. Sci. Eng. C 32 (2012) 2135–2144.
[7] F. Ren, R. Xin, X. Ge, Y. Leng, Characterization and structural analysis of zinc-substituted hydroxyapatites, Acta Biomater. 5 (2009) 3141–3149.
[8] K. Ozeki, T. Hoshino, H. Aoki, T. Masuzawa, Phase composition of sputtered film from a mixture of hydroxyapatite and strontium-apatite, J. Mater. Sci. Technol. 29 (2013) 1–6.
[9] C. O'Sullivan, P. O'Hare, N.D. O'Leary, A.M. Crean, K. Ryan, A.D.W. Dobson, L. O'Neill, Deposition of substituted apatites with anticolonizing properties onto titanium surfaces using a novel blasting process, J. Biomed. Mater. Res. B: Appl. Biomater. 95B (2010) 141–149.
[10] J.H. Shepherd, D.V. Shepherd, S.M. Best, Substituted hydroxyapatites for bone repair, J. Mater. Sci. Mater. Med. 23 (2012) 2335–2347.
[11] S. Sprio, A. Tampieri, E. Landi, M. Sandri, S. Martorana, G. Celotti, G. Logroscino, Physicochemical properties and solubility behaviour of multi-substituted hydroxyapatite powders containing silicon, Mater. Sci. Eng. C 28 (2008) 179–187.
[12] Y. Ando, H. Miyamoto, I. Noda, N. Sakurai, T. Akiyama, Y. Yonekura, T. Shimazaki, M. Miyazaki, M. Mawatari, T. Hotokebuchi, Calcium phosphate coating containing silver shows high antibacterial activity and low cytotoxicity and inhibits bacterial adhesion, Mater. Sci. Eng. C 30 (2010) 175–180.
[13] W.K. Jung, H.C. Koo, K.W. Kim, S. Shin, S.H. Kim, Y.H. Park, Antibacterial activity and mechanism of action of the silver ion in *Staphylococcus aureus* and *Escherichia coli*, Appl. Environ. Microbiol. 74 (2008) 2171–2178.
[14] M. Schierholz, L.J. Lucasj, A. Rump, G. Pulverer, Efficacy of silver-coated medical devices, J. Hosp. Infect. 40 (1998) 257–262.
[15] W.C. Chiang, L.R. Hilbert, C. Schroll, T. Tolker-Nielsen, P. Moller, Bacterial inhibiting surfaces caused by the effects of silver release and/or electrical field, Electrochim. Acta 54 (2008) 108–115.
[16] S. Seuss, M. Heinloth, A.R. Boccaccini, Development of bioactive composite coatings based on combination of PEEK, bioactive glass and Ag nanoparticles with antibacterial properties, Surf. Coat. Technol. 301 (2016) 100–105.
[17] K.M. Cheung, W.W. Lu, K.D. Luk, C.T. Wong, D. Chan, et al., Vertebroplasty by use of a strontium-containing bioactive bone cement, Spine 30 (2005) S84–S91.
[18] C.T. Wong, W.W. Lu, W.K. Chan, K.M. Cheung, K.D. Luk, D.S. Lu, A.B. Rabie, L.F. Deng, J.C. Leong, In vivo cancellous bone remodeling on a strontium-containing hydroxy apatite (Sr-HA) bioactive cement, J. Biomed. Mater. Res. 68A (2004) 513–521.
[19] G.X. Ni, W.W. Lu, K.Y. Chiu, Z.Y. Li, D.Y. Fong, K.D. Luk, Strontium-containing hydroxyapatite (Sr-HA) bioactive cement for primary hip replacement: an in vivo study, J. Biomed. Mater. Res. B: Appl. Biomater. 77 (2006) 409–415.
[20] A. Barbara, P. Delannoy, B.G. Denis, P.J. Marie, Normal matrix mineralization induced by strontium ranelatein MC3T3-E1 osteogenic cells, Metabolism 53 (2004) 532–537.
[21] J. Abert, C. Bergmann, H. Fischer, Wet chemical synthesis of strontium-substituted hydroxyapatite and its influence on the mechanical and biological properties, Ceram. Int. 40 (2014) 9195–9203.
[22] R. Baron, Y. Tsouderos, In vitro effects of S12911-2 on osteoclast function and bone marrow macrophage differentiation, Eur. J. Pharmacol. 450 (2002) 11–17.
[23] V.K. Mishra, B.N. Bhattacharjee, O. Parkash, D. Kumar, S.B. Rai, Mg-doped hydroxyapatite nanoplates for biomedical applications: a surfactant assisted microwave synthesis and spectroscopic investigations, J. Alloys Compd. 614 (2014) 283–288.
[24] D. Gopi, A. Karthika, S. Nithiya, L. Kavitha, In vitro biological performance of minerals substituted hydroxyapatite coating by pulsed electrodeposition method, Mater. Chem. Phys. 144 (2014) 75–85.
[25] H.X. Wang, S.K. Guan, X. Wang, C.X. Ren, L.G. Wang, In vitro degradation and mechanical integrity of Mg–Zn–Ca alloy coated with Ca-deficient hydroxyapatite by the pulse electrodeposition process, Acta Biomater. 6 (2010) 1743–1748.
[26] F. Marashi-Najafi, J. Khalil-Allafi, M.R. Etminanfar, Biocompatibility of hydroxyapatite coatings deposited by pulse electrodeposition technique on the Nitinol superelastic alloy, Mater. Sci. Eng. C 76 (2017) 278–286.
[27] R. Chakraborty Srijan Sengupta, P. Saha, K. Das, S. Das, Synthesis of calciumhydrogen phosphate and hydroxyapatite coating on SS316 substrate through pulsed electrodeposition, Mater. Sci. Eng. C 69 (2016) 875–883.
[28] L. Shoujie, L. Hejun, Z. Leilei, Y. Xuemin, G. Yao, In simulated body fluid performance of polymorphic apatite coatings synthesized by pulsed electrodeposition, Mater. Sci. Eng. C 79 (2017) 100–107.
[29] M. Saremi, S. Mohajernian, S. Hejazi, Controlling the degradation rate of AZ31 Magnesium alloy and purity of nano-hydroxyapatite coating by pulse electrodeposition, Mater. Lett. 129 (2014) 111–113.
[30] N. Monasterio, J.L. Ledesma, I. Aranguiz, A. Garcia-Romero, E. Zuza, Analysis of electrodeposition processes to obtain calcium phosphate layer on AZ31 alloy, Surf. Coat. Technol. 319 (2017) 12–22.
[31] T. Kokubo, H. Kushitani, S. Sakka, T. Kitsugi, T. Yamamuro, Solutions able to reproduce in vivo surface-structure changes in bioactive glass-ceramic A-W, J. Biomed. Mater. Res. 24 (1990) 721–734.
[32] L. Berzina-Cimdina, N. Borodajenco, Research of calcium phosphates using Fourier transform infrared spectroscopy, in: T. Theophile (Ed.), Infrared Spectroscopy – Materials Science Engineering and Technology, 2012, pp. 123–148, ISBN: 978-953-51-0537-4.
[33] A. Bigi, G. Falini, E. Foresti, M. Gazzano, A. Ripamonti, N. Roveri, Rietveld structure refinements of calcium hydroxylapatite containing magnesium, Acta Crystallogr. 52 (1996) 87–92.
[34] F.Z. Ren, R.L. Xin, X. Ge, Y. Leng, Characterization and structural analysis of zinc-substituted hydroxyapatites, Acta Biomater. 5 (2009) 3141–3149.
[35] Y. Cai, S. Zhang, X. Zeng, Y. Wang, M. Qian, W. Weng, Improvement of bioactivity with magnesium and fluorine ions incorporated hydroxyapatite coatings via sol–gel deposition onTi6Al4V alloys, Thin Solid Films 517 (17) (2009) 5347–5351.
[36] S. Ziani, S. Meski, H. Khireddine, Characterization of magnesium-doped hydroxyapatite prepared by sol–gel process, Int. J. Appl. Ceram. Technol. 11 (1) (2014) 83–91.
[37] Z. Geng, Z. Cui, Z. Li, S. Zhu, et al., Strontium incorporation to optimize the antibacterial and biological characteristics of silver-substituted hydroxyapatite coating, Mater. Sci. Eng. C 58 (2016) 467–477.
[38] I.C. Lavos-Valereto, I. Costa, S. Wolynec, The electrochemical behavior of Ti-6Al-7Nb alloy with and without plasma-sprayed hydroxyapatite coating in Hanks' solution, J. Biomed. Mater. Res. 63 (2002) 664–670.
[39] Z. Zhang, M.F. Dunn, T.D. Xiao, A.P. Tomsia, E. Saiz, Nanostructured hydroxyapatite coatings for improved

Please cite this article in press as: M. Furko, et al., Development and characterization of multi-element doped hydroxyapatite bioceramic coatings on metallic implants for orthopedic applications, Bol. Soc. Esp. Cerám. Vidr. (2017), http://dx.doi.org/10.1016/j.bsecv.2017.09.003

adhesion and corrosion resistance for medical implants, Nanotechnol. Biotechnol. Convers. (2002) 291–296.
[40] C.T. Kwok, P.K. Wong, F.T. Cheng, H.C. Manc, Characterization and corrosion behavior of hydroxyapatite coatings on Ti6Al4V fabricated by electrophoretic deposition, Appl. Surf. Sci. 255 (2009) 6736–6744.
[41] M. Agostini, F. Romeo, S. Inoue, M.V. Niklison-Chirou, et al., Metabolic reprogramming during neuronal differentiation, Cell Death Differ. 23 (2016) 1502–1514.
[42] L. Schneider, S. Giordano, B.R. Zelickson, et al., Differentiation of SH-SY5Y cells to a neuronal phenotype changes cellular bioenergetics and the response to oxidative stress, Free Radic. Biol. Med. 51 (11) (2011) 2007–2017.
[43] E.S. Thian, Z. Ahmad, J. Huang, M.J. Edirisinghe, S.N. Jayasinghe, D.C. Ireland, R.A. Brooks, N. Rushton, W. Bonfield, S.M. Best, The role of surface wettability and surface charge of electrosprayed nanoapatites on the behaviour of osteoblasts, Acta Biomater. 6 (2010) 750–755.
[44] K.L. Kilpadi, P.-L. Chang, S.L. Bellis, Hydroxylapatite binds more serum proteins, purified integrins, and osteoblast precursor cells than titanium or steel, J. Biomed. Mater. Res. 57 (2001) 258–267.
[45] J. Sun, L. Wei, X. Liu, J. Li, B. Li, G. Wang, F. Meng, Influences of ionic dissolution products of dicalcium silicate coating on osteoblastic proliferation, differentiation and gene expression, Acta Biomater. 5 (2009) 1284–1293.
[46] S. Zhao, Q. Jiang, S. Peel, X. Wang, F. He, Effects of magnesium-substituted nanohydroxyapatite coating on implant osseointegration, Clin. Oral Implants Res. 24 (2011) 34–41.
[47] F. Yang, W. Dong, F. He, et al., Osteoblast response to porous titanium surfaces coated with zinc substituted hydroxyapatite, Oral Surg. Oral Med. Oral Pathol. Oral Radiol. 113 (2012) 313–318.
[48] V.B. Bueno, R. Bentini, L.H. Catalani, L.R.S. Barbosa, D.F.S. Petri, Synthesis and characterization of xanthan–hydroxyapatite nanocomposites for cellular uptake, Mater. Sci. Eng. C 37 (2014) 195–203.
[49] C. Capuccini, P. Torricelli, F. Sima, E. Boanini, C. Ristoscu, B. Bracci, G. Socol, M. Fini, I.N. Mihailescu, A. Bigi, Strontium-substituted hydroxyapatite coatings synthesized by pulsed-laser deposition: in vitro osteoblast and osteoclast response, Acta Biomater. 4 (2008) 1885–1893.
[50] E.S. Thian, Z. Ahmad, J. Huang, M.J. Edirisinghe, et al., The role of electrosprayed apatite nanocrystals in guiding osteoblast behaviour, Biomaterials 29 (2008) 1833–1843.

Please cite this article in press as: M. Furko, et al., Development and characterization of multi-element doped hydroxyapatite bioceramic coatings on metallic implants for orthopedic applications, Bol. Soc. Esp. Cerám. Vidr. (2017), http://dx.doi.org/10.1016/j.bsecv.2017.09.003